

Health-Aware and User-Involved Battery Charging Management for Electric Vehicles: Linear Quadratic Strategies

Huazhen Fang, Yebin Wang, and Jian Chen

Abstract—This work studies control-theory-enabled intelligent charging management for battery systems in electric vehicles (EVs). Charging is crucial for the battery performance and life as well as a contributory factor to a user’s confidence in or anxiety about EVs. For existing practices and methods, many run with a lack of battery health awareness during charging, and none includes the user needs into the charging loop. To remedy such deficiencies, we propose to perform charging that, for the first time, allows the user to specify charging objectives and accomplish them through dynamic control, in addition to suppressing the charging-induced negative effects on battery health. Two charging strategies are developed using the linear quadratic control theory. Among them, one is based on control with fixed terminal charging state, and the other on tracking a reference charging path. They are computationally competitive, without requiring real-time constrained optimization needed in most charging techniques available in the literature. A simulation-based study demonstrates their effectiveness and potential. It is anticipated that charging with health awareness and user involvement guaranteed by the proposed strategies will bring major improvements to not only the battery longevity but also EV user satisfaction.

Index Terms—Intelligent charging, battery management, fast charging, electric vehicles, linear quadratic control, linear quadratic tracking

I. INTRODUCTION

Holding the promise for reduced fossil fuel use and air pollutant emissions, electrified transportation has been experiencing a surge of interest in recent years. Over 330,000 plug-in electric vehicles (EVs) are on the road in the United States as of May 2015 [1], with strong growth foreseeable in the coming decades. Most EVs rely on battery-based energy storage systems, which are crucial for the overall EV performance as well as consumer acceptance. Associated with this trend, the past years have witnessed a growing body of work on battery management research, e.g., state-of-charge (SoC) estimation to infer the amount of energy available in a battery, state-of-health (SoH) estimation to track the battery’s aging status, thermal monitoring to avoid

abnormal heat buildup [2]–[11]. Another essential yet less explored problem in the battery use is the charging strategies. Improper charging, e.g., charging with a high voltage or current density, can induce the rapid buildup of internal stress and resistance, crystallization and other negative effects [12]–[15]. The consequence is fast capacity fade and shortened life cycle, and even safety hazards in the extreme case, eventually impairing the consumer confidence.

Literature review: The popular charging ways, especially for inexpensive lead-acid batteries used for cars and backup power systems, are to apply a constant voltage or force a constant current flow through the battery [16]. Such methods, though easy to implement, can lead to serious detrimental effects for the battery. One improvement is the constant-current/constant-voltage charging [16], [17], which is illustrated in Figure 1. Initially, a trickle charge (0.1C or even smaller) is used for depleted cells, which produces a rise of the voltage. Then a constant current between 0.2C and 1C is applied. This stage ends when the voltage increases to a desired level. The mode then switches to constant voltage, giving a diminishing current to charge. Yet the implementation is empirical here, with the optimal determination of the charge regimes remaining in question [18]. In recent years, pulse charging has gained much interest among practitioners. Its current profile is based on pulses, as shown in Figure 2. Between two consecutive pulses is a short rest period, which allows the electrochemical reactions to stabilize by equalizing throughout the bulk of the electrode before the next charging begins. This brief relaxation can accelerate the charging process, reduce the gas reaction, inhibit dendrite growth and slow the capacity fade [19]–[21]. Its modified version, burp charging, applies a very short negative pulse for discharging during the rest period, see Figure 2, in order to remove the gas bubbles that have appeared the electrodes.

A main issue with the above methods is the lack of an effective feedback-based regulation mechanism. With an open-loop architecture, they simply take energy from power supply and put it into the battery. As a result, both the charging dynamics and the battery’s internal state are not well exploited to control the charging process for better efficiency and health protection. This motivates

H. Fang is with the Department of Mechanical Engineering, University of Kansas, Lawrence, KS 66045, USA (e-mail: fang@ku.edu).

Y. Wang is with the Mitsubishi Electric Research Laboratories, Cambridge, MA 02139, USA (e-mail: yebinwang@ieee.org).

J. Chen is with the State Key Laboratory of Industrial Control Technology and College of Control Science and Engineering, Zhejiang University, Hangzhou 310027, China (e-mail: jchen@zju.edu.cn).

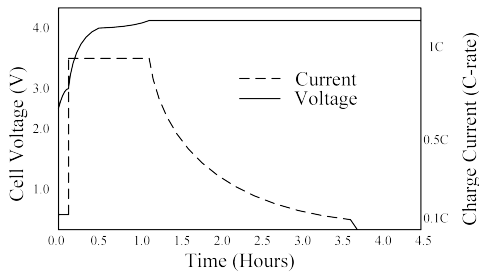


Fig. 1: Constant-current/constant-voltage charging.

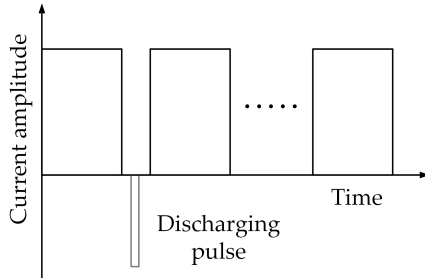


Fig. 2: Pulse charging and burp charging.

the deployment of closed-loop and model-based control. Constrained optimal control is applied in [12], [22]–[24], in conjunction with electrochemical or equivalent circuit models, to address fast charging subject to input, state and temperature constraints. In this direction, fast constrained optimization has been leveraged recently in [25], [26] to reduce the computational cost and push forward real-time charging control. With the ability of dealing with uncertain parameters, adaptive control is used for energy-efficient fast charging in [27]. Based on the Pontryagin minimum principle, optimal control design of charging/discharging is studied in [28] to maximize the work that a battery can perform over a given duration while maintaining a desired final energy level. However, we observe that the research effort for feedback-controlled charging has remained limited to date. The existing works are mostly concerned with the fast charging scenario and employ a restricted number of investigation tools, thus presenting much scope for further work.

Research motivation: In this paper, we propose to perform control-based EV charging management in a *health-aware* and *user-involved* way. Since the battery system is the heart as well as the most expensive component of an EV, health protection during charging is of remarkable importance to prevent performance and longevity degradation. As such, it has been a major design consideration in the controlled charging literature mentioned above. Furthermore, we put forward that the user involvement, entirely out of consideration in the state of the art, will bring significant improvements to charging. Two advantages at least will be created if the user can give the charging management system some commands or advisement about the charging objectives based on his/her immediate situation. The first one will

be improved battery health protection against charging-induced harm. Consider two scenarios: 1) after arriving at the work place in the morning, a user leaves the car charging at the parking point with a forecast in mind that the next drive will be in four hours; 2) he/she will have a drive to the airport in one hour, and a half full capacity will be enough. In both scenarios, the user needs can be translated into charging objectives (e.g., charge duration and target capacity). The charger then can make wiser, more health-oriented charging decisions when aiming to meet the user specifications with such information, rather than pumping, effectively but detrimentally, the maximum amount of energy into the batteries within the minimum duration. Second, a direct and positive impact on user satisfaction will result arguably, because offering a user options to meet his/her varying and immediate charging needs not only indicates a better service quality, but also enhances his/her perception of level of involvement.

Statement of contributions: We will build health-aware and user-involved charging strategies via exploring two problems. The first one is *charging with fixed terminal charging state*. In this case, the user will give target SoC and charging duration, which will be incorporated as terminal state constraint. The second problem is *tracking-based charging*, where the charging is implemented via tracking a charge trajectory. The trajectory is generated on the basis of user-specified objectives and battery health conditions. The solutions, developed in the framework of *linear quadratic optimal control*, will be presented as controlled charging laws expressed in explicit equations. The proposed methods differ from those in the literature, e.g., [12], [22]–[24], [27], [28] in either of both of the following two aspects: 1) from the viewpoint of application, they keep into account both user specifications and battery health — such a notion is unavailable before and will have a potential impact on improving the existing charging practices; 2) technically, they, though based on optimization of quadratic cost functions, do not require real-time constrained optimization needed in many existing techniques [12], [22]–[24] and thus are computationally more attractive. In addition, the linear quadratic control is a fruitful area, so future expansion of this work can be aided with many established results and new progresses, e.g., [29]–[32].

Organization: The rest of the paper is organized as follows. Section II introduces an equivalent circuit model oriented toward describing the battery charging dynamics. Section III presents the development of charging strategies. Section III-A studies the charging with fixed terminal charging state specified by the user. In Section III-B, tracking-based charging is investigated. Section IV offers numerical results to illustrate the effectiveness of the design. Finally, concluding remarks are gathered in Section V.

$$\begin{cases} \begin{bmatrix} \dot{Q}_b(t) \\ \dot{Q}_s(t) \end{bmatrix} = \begin{bmatrix} -\frac{1}{C_b(R_b + R_s)} & \frac{1}{C_s(R_b + R_s)} \\ \frac{1}{C_b(R_b + R_s)} & -\frac{1}{C_s(R_b + R_s)} \end{bmatrix} \begin{bmatrix} Q_b(t) \\ Q_s(t) \end{bmatrix} + \begin{bmatrix} \frac{R_s}{R_b + R_s} \\ \frac{R_b}{R_b + R_s} \end{bmatrix} I(t) \\ V(t) = \begin{bmatrix} R_s \\ C_b(R_b + R_s) \end{bmatrix} \begin{bmatrix} Q_b(t) \\ Q_s(t) \end{bmatrix} + \left(R_o + \frac{R_b R_s}{R_b + R_s} \right) I(t) \end{cases} \quad (1)$$

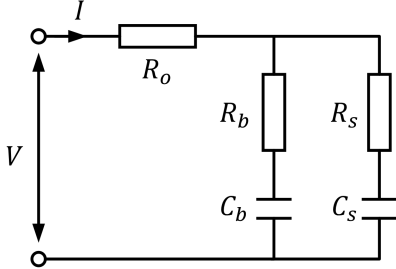


Fig. 3: The battery RC model, where R_o , R_s - C_s and R_b - C_b , respectively, simulates the resistance of the electrolyte, the surface region and the bulk inner part of an electrode.

II. CHARGING MODEL DESCRIPTION

While the energy storage within a battery results from complex electrochemical and physical processes, it has been useful to draw an analogy between the battery electrical properties and an equivalent circuit which consists of multiple linear passive elements such as resistors, capacitors, inductors and virtual voltage sources. While plenty of equivalent circuit models have been proposed, we focus our attention throughout the paper on a second-order resistance-capacitance (RC) model shown in Figure 3.

Developed by Saft Batteries, Inc., this model was intended for the simulation of battery packs in hybrid EVs [33], [34]. Identification of its parameters is discussed in [35]. As shown in Figure 3, it consists of two capacitors and three resistors. The resistor R_o represents the electrolytic resistance within a battery cell. The double RC circuits in parallel are meant to simulate the migration of the electric charge during the charging (or discharging) processes. Specifically, the R_s - C_s circuit accounts for the electrode surface region, which is exposed to the electrode-electrolyte interface; the R_b - C_b circuit represents the bulk inner part of the electrode. Seeing a fast-speed transfer of the electric charge, the electrode surface is responsible for the high-frequency behavior during the charging processes and associated with the immediate amount of charge the battery can absorb. It, however, has a rather limited storage capacity. By contrast, the bulk electrode is where the majority of the electric charge is stored in chemical form. Since the diffusion of ions within the electrode proceeds at a relatively slower speed, the R_b - C_b circuit makes up the low-frequency part of the charging response. This implies that $R_b \gg R_s$ and $C_b \gg C_s$. Note that it has been a significant effort to use the RC circuits to approximate

electrochemical processes at different scales of time and frequency [36], [37]. The state-space representation of the model is shown in (1). It can be verified that this system is controllable and observable, indicating the feasibility of both controlled charging and state monitoring.

Based on the model, the overall SoC is given by

$$\text{SoC} = \frac{Q_b - \underline{Q}_b + Q_s - \underline{Q}_s}{\bar{Q}_b - \underline{Q}_b + \bar{Q}_s - \underline{Q}_s}, \quad (2)$$

where \underline{Q}_j and \bar{Q}_j for $j = b, s$ denote the minimum and the maximum allowed charge held by the capacitor C_j , which represent the operating limits of the battery. When the equilibrium $V_b = V_s$ is reached, the SoC can be simply expressed as the linear combination of SoC_b and SoC_s , i.e.,

$$\text{SoC} = \frac{C_b}{C_b + C_s} \text{SoC}_b + \frac{C_s}{C_b + C_s} \text{SoC}_s. \quad (3)$$

The RC model can well grasp the ‘‘rate capacity effect’’, which means that the total charge absorbed by a battery goes down with the increase in charging current as is often stated as the Peukert’s law. To see this, consider that a positive current is applied for charging. Then both Q_b and Q_s , and their voltages, V_b and V_s , will grow. However, V_s increases at a rate faster than V_b . When the current I is large, the terminal voltage V , which is largely dependent on the fast increasing V_s , will grow quickly as a result. Then V will reach the cut-off threshold in a short time. This will have the charging process terminated, though Q_b still remains at a low level. Another essential phenomenon that can be well approximated by this RC model is the ‘‘recovery effect’’. upon an interruption of charging. That is, when the charging stops, the terminal voltage V will see a transient decrease due to the charge transfer from C_s to C_b .

To develop a digitally controlled charging scheme, the model in (1) is discretized with a sampling period of t_s . The discrete-time model takes the following standard form:

$$\begin{cases} x_{k+1} = Ax_k + Bu_k \\ y_k = Cx_k + Du_k \end{cases} \quad (4)$$

where $x = [Q_b \quad Q_s]^\top$, $u = I$, $y = V$, and A , B , C and D can be decided according to the discretization method applied to (1).

Despite being linear and straightforward, the above RC model can satisfy the practical needs in many applications. This is because battery systems, e.g., those

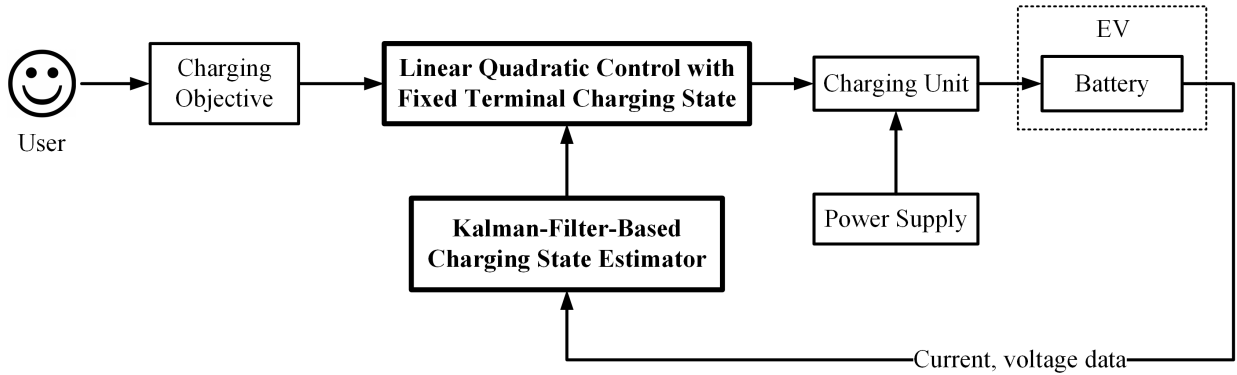


Fig. 4: The schematic diagram for charging based on linear quadratic control with fixed terminal charging state.

in electric vehicles, need to limit the minimum and maximum SoC during operation [38], [39] for the purposes of safety, life, and a consistent power capability. Within this favorable SoC range, the battery behavior can be approximated as linear due to battery open-circuit-voltage profiles.

For health consideration, we need to constrain the difference between voltages across C_s and C_b , denoted as V_s and V_b respectively, throughout the charging process. Note that $V_s - V_b$ is the force that drives the migration of the charge from C_s to C_b during charging. It shares great resemblance with the gradient of the concentration of Li ions within the electrode created during charging causing the diffusion of ions. This observation is further investigated in the Appendix, where the analogy between the voltage difference and the Li-ion concentration gradient is validated through a proof approximate equivalence between the model in (1) and the well-known single particle model (SPM) under certain conditions. Too large a gradient value will cause internal stress increase, heating, solid-electrolyte interphase (SEI) formation and other negative side effects [40]–[42]. Mechanical degradation in the electrode and capacity fade will consequently happen. Thus to reduce the battery health risk, non-uniformity of the ion concentration should be suppressed during charging, and this implies the necessity of suppressing the voltage difference. It is also noteworthy that such a restriction should be implemented more strictly as the SoC increases, because the adverse effects of a large concentration difference on the battery would be stronger then.

Next, we will build the charging strategies on the basis of the above RC model. The development will be laid out in the framework of linear quadratic control, taking into account both health awareness and user needs.

III. HEALTH-AWARE AND USER-INVOLVED CHARGING STRATEGIES

In this section, we will develop two charging strategies. For both, the user specifies the desired charging duration and target capacity. The first strategy accomplishes the task via a treatment based on linear quadratic

control subject to fixed terminal state resulting from the user objective. In the second case, charging is managed via tracking a charging trajectory which is produced from the user objective. A discussion of the strategies will follow.

A. Charging with Fixed Terminal Charging State

A charging scenario that frequently arises is: according to the next drive need, a user will inform the charging management system of his/her objective in terms of target SoC and charging duration. This can occur for overnight parking at home and daytime parking at the workplace, or when a drive to some place will set off in a predictable time. As afore discussed, the objective offered by the user, if incorporated into the dynamic charging decision making process, would create benefits for health protection compared to fast charging. This motivates us to propose a control-enabled charging system illustrated in Figure 4. The charging objective given by the user is taken and translated into the desired terminal charging state. A linear quadratic controller will compute online the charging current to apply so as to achieve the target state when the charging ends. Meanwhile, a charging state estimator will monitor the battery status using the current and voltage measurements, and feed the information to the controller. In the following, we will present how to realize the above charging control.

From the perspective of control design, the considered charging task can be formulated as an optimal control problem, which minimizes a cost function commensurate with the harm to health and subject to the user's goal. With the model in (4), the following linear quadratic control problem will be of interest:

$$\begin{aligned} \min_{u_0, u_1, \dots, u_{N-1}} & \frac{1}{2} x_N^\top S_N x_N \\ & + \frac{1}{2} \sum_{k=0}^{N-1} \left(x_k^\top G^\top Q_k G x_k + u_k^\top R u_k \right), \quad (5) \\ \text{subject to} & x_{k+1} = A x_k + B u_k, \quad x_0 \\ & x_N = \bar{x}. \end{aligned}$$

where $S_N \geq 0$, $Q_k \geq 0$, $R > 0$ and

$$G = \begin{bmatrix} -\frac{1}{C_b} & \frac{1}{C_s} \end{bmatrix}.$$

In above, Gx_k represents the potential difference between C_b and C_s , and the time range N and the final state \bar{x} are generated from the user-specified charging duration and target SoC. Note that the battery should be at the equilibrium point with $V_b = V_s$ in the final state and that using (2)-(3), \bar{x} can be easily determined from the specified SoC value. The quadratic cost function thus intends to constrain the potential difference and magnitude of the charging current during the charging process. The minimization is subject to both the state equation and the fixed terminal state. The weight coefficient Q_k should be chosen in a way such that it increases over time, in order to offer stronger health protection that is needed as the SoC builds up. It is noted that $x_N^T S_N x_N$ represents a general formulation of the terminal cost, to which different options can be assigned. It vanishes, for example, if $S_N = 0$. Or it can be set as $S_N = G^T Q_N G$ to constrain the voltage difference in the end state. However, since subjected to the hard constraint $x_N = \bar{x}$, the end state would reach the desired point regardless of S_N .

Resolving the problem in (5) will lead to a state-feedback-based charging strategy, which can be expressed in a closed-form [29]:

$$K_k = (B^T S_N B + R)^{-1} B^T S_{k+1} A, \quad (6)$$

$$S_k = A^T S_{k+1} (A - BK_k) + Q_k, \quad (7)$$

$$T_k = (A - BK_k)^T T_{k+1}, \quad T_N = I, \quad (8)$$

$$P_k = P_{k+1} - T_{k+1}^T B (B^T S_{k+1} B + R)^{-1} B^T T_{k+1}, \quad (9)$$

$$P_N = 0, \quad (9)$$

$$K_k^u = (B^T S_{k+1} B + R)^{-1} B^T, \quad (10)$$

$$u_k = - \left(K_k - K_k^u T_{k+1} P_k^{-1} T_k^T \right) x_k - K_k^u T_{k+1} P_k^{-1} \bar{x}. \quad (11)$$

This procedure comprises offline backward computation of the matrices K_k , S_k , T_k , P_k and K_k^u from the terminal state and online forward computation of the control input (i.e., charging current) u_k .

The state variable x_k is not measurable directly in practice, so its real-world application necessitates the conversion of the above state-feedback-based strategy to an output-feedback-based one. One straightforward avenue to achieve this is to replace x_k by its prediction \hat{x}_k . This is justifiable by the certainty equivalence principle, which allows the optimal output-feedback control design to be divided into the separate designs of an optimal state-feedback control and an optimal estimator [43]. The optimal estimation can be treated via minimizing

$$\min_{x_0, x_1, \dots, x_k} \frac{1}{2} (x_0 - \hat{x}_0)^T \Sigma_0^{-1} (x_0 - \hat{x}_0)$$

$$+ \frac{1}{2} \sum_{i=0}^{k-1} w_i^T \Pi^{-1} w_i + \frac{1}{2} \sum_{i=0}^k v_i^T \Lambda^{-1} v_i, \quad (12)$$

where $\Sigma_0 > 0$, $\Pi > 0$, $\Lambda > 0$, and

$$w_k = x_{k+1} - Ax_k - Bu_k,$$

$$v_k = y_k - Cx_k - Du_k.$$

The one-step-forward Kalman predictor will result from solving (12), which is given by

$$L_k = A \Sigma_k C^T (C \Sigma_k C^T + \Lambda)^{-1}, \quad (13)$$

$$\hat{x}_{k+1} = A \hat{x}_k + Bu_k + L_k (y_k - C \hat{x}_k - Du_k), \quad (14)$$

$$\Sigma_{k+1} = A \Sigma_k A^T + \Pi - A \Sigma_k C^T \cdot (C \Sigma_k C^T + \Lambda)^{-1} C \Sigma_k A^T. \quad (15)$$

Substituting x_k with its estimate \hat{x}_k , the optimal control law in (11) will become

$$u_k = - \left(K_k - K_k^u T_{k+1} P_k^{-1} T_k^T \right) \hat{x}_k - K_k^u T_{k+1} P_k^{-1} \bar{x}. \quad (16)$$

Putting together (6)-(10), (13)-(15) and (16), we will obtain a complete description of the charging method via linear quadratic control with fixed terminal state, which is named LQCwFSTS and summarized in Table I. The LQCwFSTS method performs state prediction at each time instant, and then feeds the predicted value, which is a timely update about the battery's internal state, to generate the control input to charge the battery. Much of the computation for LQCwFSTS can be performed prior to the implementation of the control law. The sequences, K_k , S_k , T_k , P_k and K_k^u can be computed offline, and then K_k , $K_k^u T_{k+1} P_k^{-1} T_k^T$ and $K_k^u T_{k+1} P_k^{-1}$ are stored for use when the control is applied. On the side of the Kalman prediction, offline computation and storage of L_k can be done. Then the only work to do during charging is to compute the optimal state prediction and control input by (14) and (16), reducing the computational burden.

B. Charging Based on Tracking

Tracking-control-based charging is another way to guarantee health awareness and user objective satisfaction. A schematic of its realization is shown in Figure 5. When a user specifies the charging objective, a charging trajectory can be generated. A charging controller will be in place to track the path. The trajectory generation will be conducted with a mix of prior knowledge of the battery electrochemistries, health awareness and user needs. It is arguably realistic that an EV manufacturer can embed trajectory generation algorithms into BMSs mounted on EVs, from which the user can select the one that best fits the needs when he/she intends to charge the EV. Leaving optimal charging trajectory generation for our future quest, we narrow our attention to the focus of path-tracking-based charging control here.

Suppose that the user describes the target SoC and duration for charging, which are translated into the final state \bar{x} . Then a reference trajectory r_k for $k = 0, 1, \dots, N$ is calculated with $r_N = \bar{x}$. Note that the trajectory should

<p>Offline backward computation (from time N to 0)</p> $K_k = (B^\top S_N B + R)^{-1} B^\top S_{k+1} A$ $S_k = A^\top S_{k+1} (A - BK_k) + Q_k$ $T_k = (A - BK_k)^\top T_{k+1}, T_N = I$ $P_k = P_{k+1} - T_{k+1}^\top B (B^\top S_{k+1} B + R)^{-1} B^\top T_{k+1}, P_N = 0$ $K_k^u = (B^\top S_{k+1} B + R)^{-1} B^\top$
<p>Online forward computation (from time 0 to N)</p> <p><i>Battery state prediction</i></p> $L_k = A \Sigma_k C^\top (C \Sigma_k C^\top + \Lambda)^{-1}$ $\hat{x}_{k+1} = A \hat{x}_k + B u_k + L_k (y_k - C \hat{x}_k - D u_k)$ $\Sigma_{k+1} = A \Sigma_k A^\top + \Pi - A \Sigma_k C^\top (C \Sigma_k C^\top + \Lambda)^{-1} C \Sigma_k A^\top$ <p><i>Charging decision</i></p> $u_k = - \left(K_k - K_k^u T_{k+1} P_k^{-1} T_k^\top \right) \hat{x}_k - K_k^u T_{k+1} P_k^{-1} \bar{x}$

TABLE I: The LQCwFTS charging strategy (Linear Quadratic Control with Fixed Terminal State).

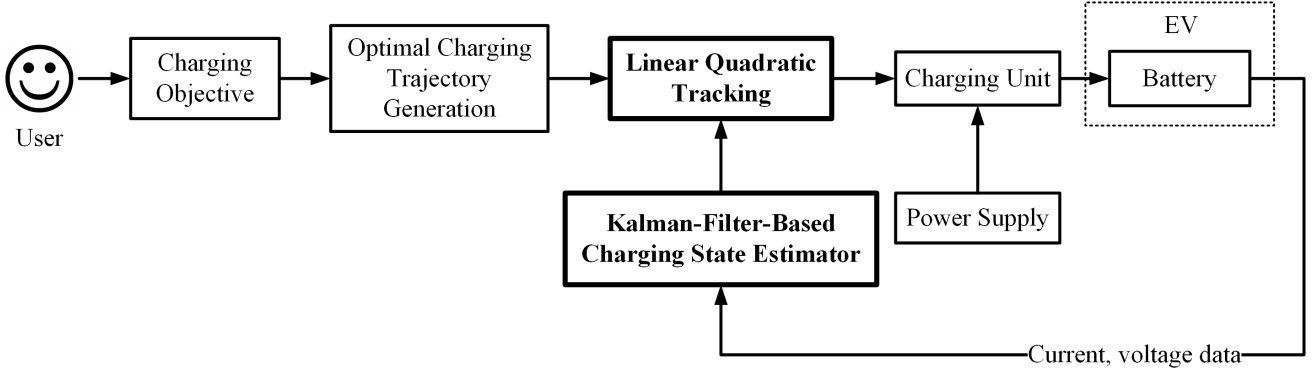


Fig. 5: The schematic diagram for charging based on linear quadratic tracking.

constrain the difference between V_b and V_s to guarantee health. A linear quadratic state-feedback tracking can be considered for charging:

$$\begin{aligned} & \min_{u_0, u_1, \dots, u_{N-1}} \frac{1}{2} (x_N - r_N)^\top S_N (x_N - r_N) \\ & + \frac{1}{2} \sum_{k=0}^{N-1} \left[(x_k - r_k)^\top Q (x_k - r_k) + u_k^\top R u_k \right], \quad (17) \\ & \text{subject to } x_{k+1} = A x_k + B u_k, x_0 \end{aligned}$$

where $S_N \geq 0$, $Q \geq 0$ and $R > 0$. Referring to [29], the optimal solution to the above problem is expressed as follows:

$$K_k = (B^\top S_{k+1} B + R)^{-1} B^\top S_{k+1} A, \quad (18)$$

$$K_k^s = (B^\top S_{k+1} B + R)^{-1} B^\top, \quad (19)$$

$$S_k = A^\top S_{k+1} (A - BK_k) + Q, \quad (20)$$

$$s_k = (A - BK_k)^\top s_{k+1} + Q r_k, s_N = S_N r_N, \quad (21)$$

$$u_k = -K_k x_k + K_k^s s_{k+1}. \quad (22)$$

Resembling (6)-(11), the execution of the above proce-

dures is in a backward-forward manner. Specifically, (18)-(21) are computed offline and backward prior to charging, and (22) online and forward from the moment when charging begins.

Following lines analogous to the development of LQCwFTS, the output-feedback tracker for charging can be created based on (18)-(22) running with the Kalman predictor in (13)-(15). That is, (22) will use \hat{x}_k rather than x_k in practical implementation, i.e.,

$$u_k = -K_k \hat{x}_k + K_k^s s_{k+1}. \quad (23)$$

Summarizing (18)-(21), (13)-(15) and (23) will yield the linear quadratic tracking strategy, or LQT, for charging, see Table II. Similar to the aforeproposed LQCwFTS, the LQT can have much computation completed offline. Then only the Kalman state prediction and optimal tracking control (23) need to be computed during the actual control run.

The computational cost of LQT can be further reduced if we use its steady-state counterpart, making it more desirable in the charging application. The steady-state tracker is deduced as follows. It is known that, if (A, B) is

<p>Offline backward computation (from time N to 0)</p> $K_k = (B^\top S_{k+1} B + R)^{-1} B^\top S_{k+1} A$ $K_k^s = (B^\top S_{k+1} B + R)^{-1} B^\top$ $S_k = A^\top S_{k+1} (A - BK_k) + Q$ $s_k = (A - BK_k)^\top s_{k+1} + Qr_k, \quad s_N = S_N r_N$
<p>Online forward computation (from time 0 to N)</p> <p><i>Battery state prediction</i></p> $L_k = A \Sigma_k C^\top (C \Sigma_k C^\top + \Lambda)^{-1}$ $\hat{x}_{k+1} = A \hat{x}_k + B u_k + L_k (y_k - C \hat{x}_k - D u_k)$ $\Sigma_{k+1} = A \Sigma_k A^\top + \Pi - A \Sigma_k C^\top (C \Sigma_k C^\top + \Lambda)^{-1} C \Sigma_k A^\top$ <p><i>Charging decision</i></p> $u_k = -K_k \hat{x}_k + K_k^s s_{k+1}$

TABLE II: The LQT charging strategy (Linear Quadratic Tracking).

<p>Offline computation of DAREs and gains</p> $S = A^\top S A - A^\top S B (B^\top S B + R)^{-1} B^\top S A + Q$ $\Sigma = A \Sigma A^\top - A \Sigma C^\top (C \Sigma C^\top + \Lambda)^{-1} C \Sigma A^\top + \Pi$ $\bar{K} = (B^\top S B + R)^{-1} B^\top S A$ $\bar{K}^s = (B^\top S B + R)^{-1} B^\top$ $\bar{L} = A \Sigma C^\top (C \Sigma C^\top + \Lambda)^{-1}$
<p>Offline computation of s_0 (from time N to 0)</p> $s_k = (A - B \bar{K})^\top s_{k+1} + Qr_k, \quad s_N = S_N r_N$
<p>Online forward computation (from time 0 to N)</p> <p><i>Battery state prediction</i></p> $\hat{x}_{k+1} = A \hat{x}_k + B u_k + \bar{L} (y_k - C \hat{x}_k - D u_k)$ <p><i>Charging decision</i></p> $s_{k+1} = (A - B \bar{K})^{-\top} s_k - (A - B \bar{K})^{-\top} Qr_k$ $u_k = -\bar{K} \hat{x}_k + \bar{K}^s s_{k+1}$

TABLE III: The SS-LQT charging strategy (Steady-State Linear Quadratic Tracking).

stabilizable and $(A, Q^{\frac{1}{2}})$ is detectable, S_k , as $N - k \rightarrow \infty$, will approach a unique stabilizing solution of the discrete algebraic Riccati equation (DARE)

$$S = A^\top S A - A^\top S B (B^\top S B + R)^{-1} B^\top S A + Q.$$

Then K_k and K_k^s will approach their respective steady-state values, \bar{K} and \bar{K}^s . In a similar way, the Kalman gain L_k will achieve steady state \bar{L} as $k \rightarrow \infty$ given the detectability of (A, C) and stabilizability of $(A, Q^{\frac{1}{2}})$, which is the unique stabilizing solution to the DARE

$$\Sigma = A \Sigma A^\top - A \Sigma C^\top (C \Sigma C^\top + \Lambda)^{-1} C \Sigma A^\top + \Pi.$$

According to the DARE theory, S and Σ can be solved for analytically. With the steady-state gains \bar{K} , \bar{K}^s and \bar{L} ,

the optimal prediction and control for charging will be

$$u_k = -\bar{K} \hat{x}_k + \bar{K}^s s_{k+1}, \quad (24)$$

$$\hat{x}_{k+1} = A \hat{x}_k + B u_k + \bar{L} (y_k - C \hat{x}_k - D u_k). \quad (25)$$

If $(A - B \bar{K})$ is invertible, the backward computation of s_k can be substituted by the forward computation governed by

$$s_{k+1} = (A - B \bar{K})^{-\top} s_k - (A - B \bar{K})^{-\top} Qr_k. \quad (26)$$

Its implementation is initialized by s_0 computed offline by (21). We refer to this suboptimal charging strategy (24)-(26) as the steady-state LQT, or SS-LQT and outline it in Table III. The SS-LQT strategy, due to its exceptional simplicity, has more computational appeal

in terms of time and space complexity.

C. Discussion

The following remarks summarize our discussion of the proposed charging strategies.

Remark 1: (Soft-constraint-based health awareness). As is seen, the proposed LQCwFTS, LQT and SS-LQT strategies incorporate the health awareness as part of the cost functions rather than hard constraints. This soft-constraint-based treatment will bring the primary benefit of computational efficiency and convenience. This compares with the techniques based on real-time constrained optimization, which are relatively more time-consuming and on occasions, face the issue that no feasible solution exists in the constrained region. In the meantime, soft constraints are acknowledged as less powerful than hard constraints, e.g., [12], [22]–[26], in terms of preventing violation of certain physical limits during charging. However, we argue that the use of soft constraints does not compromise the effectiveness of the proposed strategies to protect the battery health. This is fundamentally because the usual cause of an actual limit violation is too aggressive a charging current and an essential part of the proposed strategies is to suppress the magnitude of the charging current. For instance, it is noted that the harm to health is associated with a weighted penalty for the LQCwFTS. When a proper weight Q_k is selected, minimizing the penalty cost will ensure a sufficient consciousness of the health.

Remark 2: (Robustness of SS-LQT). The SS-LQT strategy is based on a combination of linear quadratic tracker and a Kalman filter. Such a design may engender weak robustness in terms of gain and phase margins. To overcome this limitation, the loop transfer recovery can be used to build robust control design on the linear quadratic control structure [29].

Remark 3: (Choice of Q_k and R for LQCwFTS). When the weight coefficients Q_k and R take different values, the charging profiles generated by the LQCwFTS strategy will change accordingly. This implies the importance of finding appropriate Q_k or R for the implementation. A basic guideline is as follows:

- Q_k should increase over time to suppress the use of a large current when SoC becomes larger, because of a battery's susceptibility increasing with SoC to the charging current.
- $Q_k \gg R$, because the Q -weighted term in J is much smaller than the R -weighted term.
- The larger Q_k is, the less aggressive charging action will be. However, the overall charging action also depends on the final state constraint.

It should be noted that the selection of α and β is a multi-faceted issue, because it needs to account for both battery health protection and charging speed and more broadly, the economic cost and user satisfaction. Since these factors depend on specific application scenarios,

we leave this issue for practitioners to resolve based on the above guideline.

Remark 4: (Generality to other models). The proposed development has a potential applicability to other battery models. First, the investigation, though based on a linear model, can be extended to nonlinear battery models. It is observed that, for various control-oriented battery models, the nonlinearity exists only in measurement equation that relates the state and applied current with the measured output voltage. Thus, an extension can be readily made by deploying a nonlinear Kalman filter for state estimation without changing the control structure. We can also generalize the design to the well-known single particle model (SPM). This model represents each battery electrode as a spherical particle and delineates the migration of ions in and between the particles as a diffusion process [44]. The PDE-based SPM can be converted into the standard linear state-space form, as shown in [2]. Then following similar lines to this work, linear quadratic problems can be established and solved for charging tasks, where the difference of ion concentration gradients are constrained to penalize charging-induced harm. It is also worth pointing out that extensions can be made to accommodate the temperature dynamics as a means to suppress the charging-induced heat build-up. Specifically for the considered model in Equation (1), a thermal coupling can be performed as shown in [35]. We can then follow similar lines to accomplish the linear quadratic charging design based on the modified model.

IV. NUMERICAL ILLUSTRATION

In this section, we present two simulation examples to illustrate the performance of the proposed charging strategies. Let us consider a lithium-ion battery described by the RC model in (1) with known parameters provided by Saft Inc. for hybrid electric vehicles, with $C_b = 82$ kF, $R_b = 1.1$ m Ω , $C_s = 4.074$ kF, $R_s = 0.4$ m Ω , and $R_o = 1.2$ m Ω [33]. It has a nominal capacity of 7 Ah. The model is discretized by a sampling period of $t_s = 1$ s. The initial SoC is assumed to be 30%. The user will specify that certain SoC must be achieved within certain duration.

Example 1 - Application of LQCwFTS: Suppose that the user wants to complete the charging in 2 hours. The total number of time instants thus is $N = 7200$. Meanwhile, he/she specifies the target SoC value. For the simulation purpose, different target SoC values, 55%, 65%, 75%, 85% and 95%, are set here. We apply the LQCwFTS method to carry out the charging tasks. For the control run, $Q_k = 0.1 \cdot (5 \times 10^7)^{k/N}$ and $R = 0.1$. The exponential increase of Q_k is due to the growing vulnerability of the battery to a larger charging current when the SoC increases. The practical system will be subject to certain noises, the covariances of which should be included in the Kalman filter implementation. Here, we assume that $W = 10^{-4}I$ and $V = 10^{-4}$.

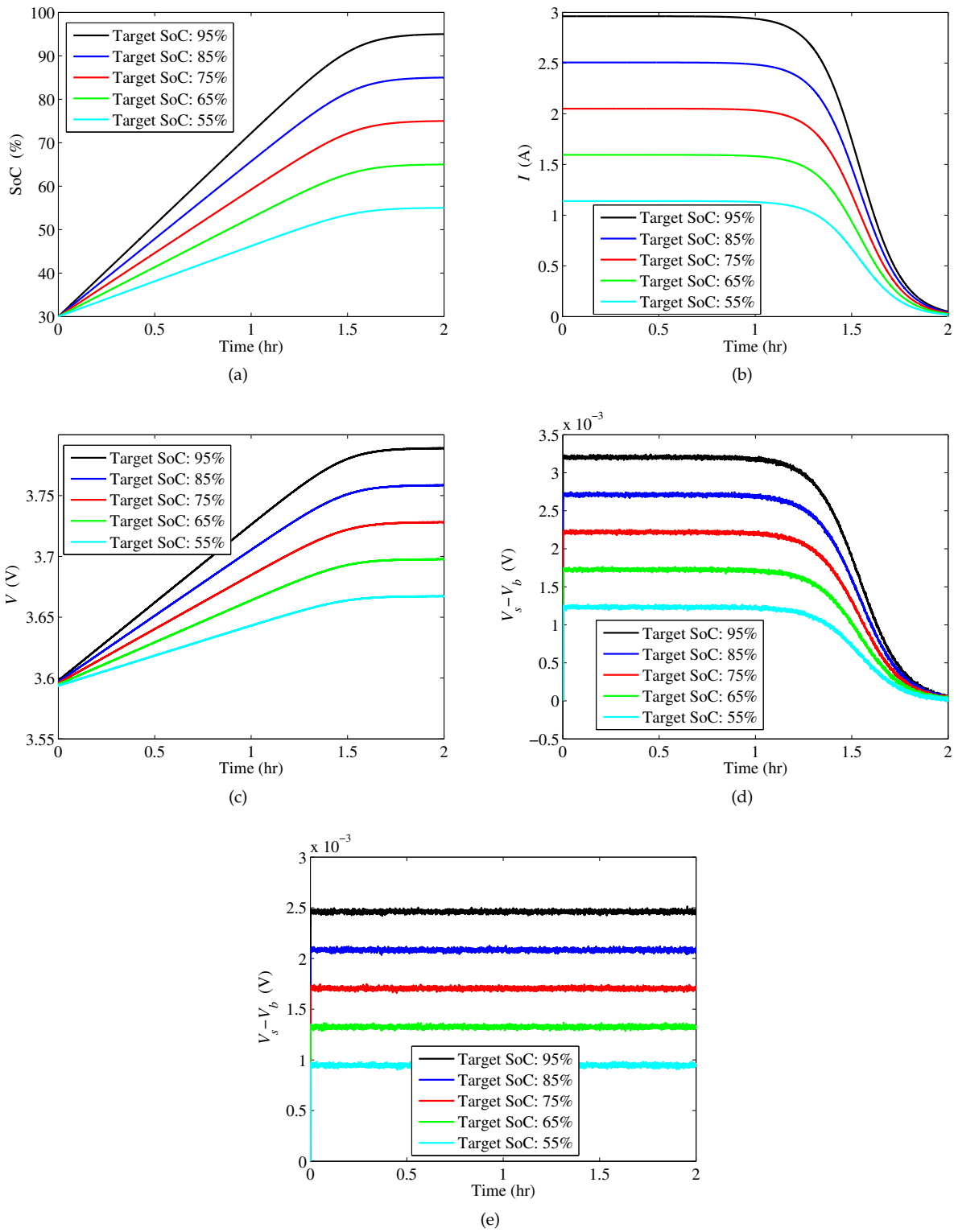


Fig. 6: Example 1 - Application of LQCwFTS to charge the battery from an initial SoC at 30% to 55%, 65%, 75%, 85% and 95%: (a) the SoC trajectories over time; (b) the charging current profiles; (c) the output voltage profiles; (d) the potential differences as health indicator; (e) potential difference due to constant current charging.

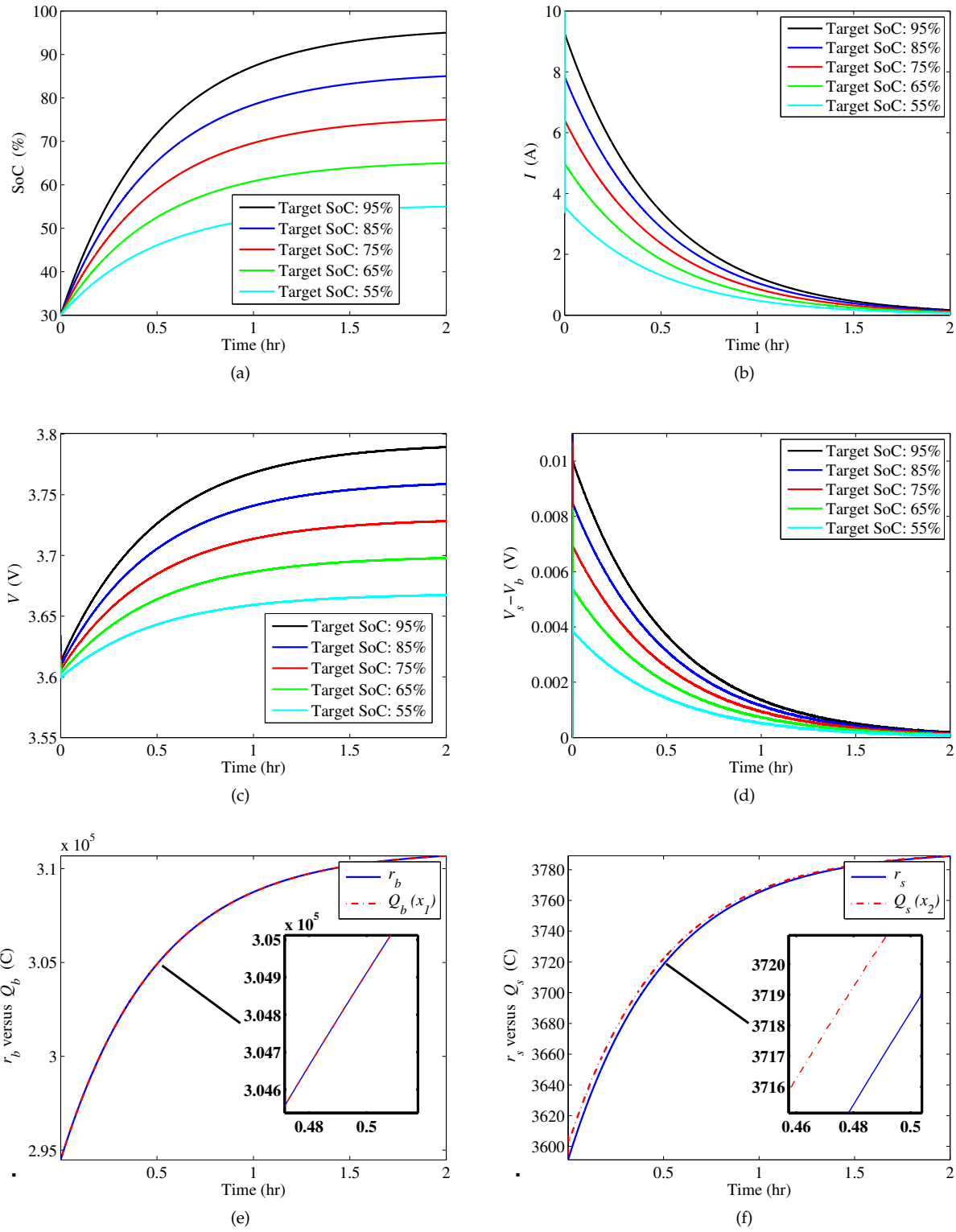


Fig. 7: Example 2 - Application of LQT to charge the battery from 30% to 55%, 65%, 75%, 85% and 95%: (a) the SoC trajectories over time; (b) the charging current profiles; (c) the output voltage profiles; (d) the potential differences; (e) tracking of x_1 (i.e., Q_b) for 95% target SoC; (f) tracking of x_2 (i.e., Q_s) for 95% target SoC.

The computational results are illustrated in Figure 6. It is shown in Figure 6a that the different target SoCs are satisfied when the charging ends right after two hours, meeting the user-specified objectives. The SoC increases approximately proportionally with time for the first 1.25 hours. Then the rate slows down gradually to zero as the charging objective is being approached. This results from a much larger weight Q_k in the later stage for health protection. The charging current is kept at almost a constant level initially during each charging implementation, as illustrated in Figure 6b. For a higher target SoC, the magnitude of the current is larger accordingly. However, the current drops quickly in each case as the SoC grows further. The profiles of the corresponding output voltage is shown in Figure 6c. They in general follow a similar trend with the SoC trajectories, rising steadily at first and then at gradually declining rates. The voltage difference between C_s and C_b , which quantifies the harm incurred to the battery, is characterized in Figure 6d. In each case, $V_s - V_b$ remains around a constant value in the first hour, despite high-frequency fluctuations due to noise. This is because a battery can accept a higher current at a low SoC level. Yet the differences decreases drastically as more charge is sent into the battery, in order to maximize the health of the battery's internal structure. For comparison, we enforce a constant current of appropriate magnitude to flow through the battery for 2 hours to reach the desired SoC. The consequent potential differences are shown in Figure 6e, which are kept at a fixed level unsurprisingly. This, however, will cause much more detrimental effects to the battery when SoC grows, thus expediting the aging processes.

Example 2 - Application of SS-LQT: We consider the use of SS-LQT for charging in this example, which is an upgraded version of LQT but more computationally efficient. The problem setting and the tasks are the same as in Example 1 — charging the battery from an SoC of 30% to 55%, 65%, 75%, 85% and 95% in 2 hours for the same battery. The charging trajectory is generated based on the task. For simplicity and convenience, we assume that the desired trajectories for x_1 and x_2 , denoted as r_b and r_s , are generated by

$$r_{j,k} = \frac{1 - e^{-kt_s/\tau_j}}{1 - e^{-Nt_s/\tau_j}}(r_{j,N} - r_{j,0}) + r_{j,0},$$

where $j = b$ or s , $k = 1, 2, \dots, N - 1$ and $r_{j,0}$ is the initial charge, $r_{j,N}$ the target charge, and τ_j the time coefficient for $j = b$ or s . Note that $r_{j,0}$ and that $r_{j,N}$ can be calculated from the initial SoC and user-specified target SoC. The resultant trajectories have a steep increase followed by a gentle slope, which are reasonable in view of health protection. Letting $\tau_b = \tau_s = Nt_s/4$, V_s and V_b are forced to be equal through the charging process. Thus at the trajectory design stage, we put the minimization of the detrimental effects well into consideration.

With the reference trajectories generated, the SS-LQT strategy is applied to charging. The actual SoC increase

over time is demonstrated in Figure 7a. All the targets are reached. In each case, the SoC grows at a fast rate when the SoC is at a low level but at a slower rate when the SoC becomes higher. Figure 7b shows the current produced by SS-LQT. The current usually begins with a large magnitude but decreases quickly. Figure 7c demonstrates the output voltage profiles of the battery, which see a progressively decelerating growth. The potential difference, given in Figure 7d, has a similar trend to the current profiles. It is relatively high when the charging starts, and then reduces fast. The state tracking for the task of 95% SoC is shown in Figures 7e and 7f. It is observed that tracking of r_b by x_1 exhibits high accuracy. Tracking of r_s by x_2 , however, is increasingly accurate, despite a minor deviation in the first hour. Overall, the closer the target SoC is approached, the smaller the tracking error becomes.

In the above examples, different charging current profiles are generated for the same charging task. While the contributory factors include the selection of Q and the reference charging trajectory generation, such a difference poses another important question: how to assess and compare the charging strategies? There is no clear-cut answer yet as it involves a mix of battery electrochemistry, charging performance, computational complexity, economic cost, and even user satisfaction. Though beyond scope of this paper, evaluation of charging strategies through theoretical analysis and experimental validation will be part of our future quest.

V. CONCLUSIONS

Effective battery charging management is vital for the development of EVs. Recently, fast charging control has attracted some research effort. However, the problem of health-aware and user-involved charging has not been explored in the literature. In this paper, we propose a set of first-of-its-kind charging strategies, which aim to meet user-defined charging objectives with awareness of the hazards to health. They are developed in the framework of linear quadratic control. One of them is built on control with fixed terminal state, and the other two on tracking a reference charging trajectory. In addition to the merits of health consciousness and user involvement, they are more computationally competitive than most existing charging techniques requiring online real-time optimization solvers. The usefulness of the proposed strategies is evaluated via a simulation study. This work will provide further incentives for research on EV charging management and is also applicable to other battery-powered applications such as consumer electronics devices and renewable energy systems. Our future research will include battery-type-specific voltage difference limit identification, optimal charging trajectory generation, and a comprehensive assessment of the charging strategies.

APPENDIX

ON APPROXIMATE EQUIVALENCE BETWEEN (1) AND SPM

This appendix is to present a proof of approximate mathematical equivalence between the RC model in (1) and the SPM. This will demonstrate that the difference in voltages across C_b and C_s in Figure 3 approximates the Li-ion concentration gradient in the SPM.

The SPM simplifies each electrode as a spherical particle with area equivalent to the active area of this electrode [45]. Striking a balance between mathematical complexity and fidelity toward capturing key physical and electrochemical phenomena, it has found significant use in the study battery management, e.g., [2], [3], [10]. At the core of the SPM is the conservation of Li ions in the electrode phase. Specifically, the migration of Li ions inside a solid particle is caused by the gradient-induced diffusion. It follows from the Fick's laws of diffusion that

$$\frac{\partial c_j(r,t)}{\partial t} = \frac{1}{r^2} \frac{\partial}{\partial r} \left(D_j r^2 \frac{\partial c_j(r,t)}{\partial r} \right), \quad (\text{A.1})$$

where c is the concentration of Li ions in the solid electrode, D the diffusion coefficient, r the radial dimension of the spherical particle representing the electrode, and $j = n, p$ with n for the negative electrode and p for the positive one. The associated initial and boundary conditions are given by

$$c_j(r,0) = c^0, \quad \frac{\partial c_j}{\partial r} \Big|_{r=0} = 0, \quad \frac{\partial c_j}{\partial r} \Big|_{r=R_j} = -\frac{1}{D_{s,j}} J_j. \quad (\text{A.2})$$

Here, J_j is the molar flux at the electrode/electrolyte interface of a single particle. When $j = n$ and p , respectively,

$$J_n(t) = -\frac{I(t)}{FS_n}, \quad J_p(t) = \frac{I(t)}{FS_p}, \quad (\text{A.3})$$

where I is the charging ($I > 0$) or discharging ($I < 0$) current, S the surface area, and R_j the radius of the particle.

Next, we consider convert the PDE-based diffusion equation into a system of ODE equations using a finite-volume approach. That is, we subdivide the particle along the radial coordinate into a set of continuous finite volumes, as shown in Figure 8a. The finite volume at the center is a ball with a radius r_0 , and the rest hollow spheres. The i -th sphere for $i = 0, 1, \dots, N$ has an outer radius of r_i with $r_N = R$. Note that $r_{-1} = 0$.

The total Li-ion amount within the i -th finite volume can be quantified as

$$\begin{aligned} Q_{j,i}(t) &= \int_{r_{i-1}}^{r_i} c_j(r,t) dV \\ &= \int_{r_{i-1}}^{r_i} c_j(r,t) \cdot 4\pi r^2 dr. \end{aligned} \quad (\text{A.4})$$

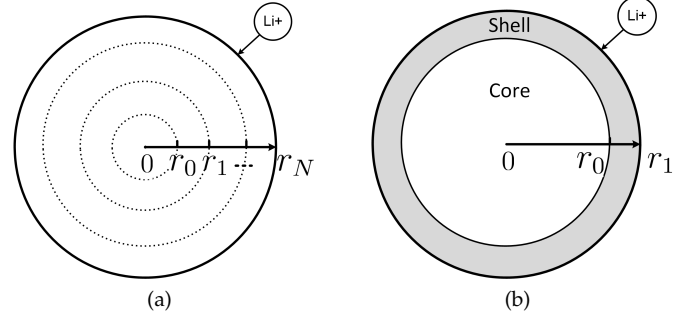


Fig. 8: (a) Subdivision of the spherical particle representing the positive electrode into multiple finite volumes along the radial coordinate; (b) subdivision of the particle into two finite volumes, named the core and shell, respectively.

Inserting (A.1) into (A.4), we have

$$\begin{aligned} \dot{Q}_{j,i}(t) &= \int_{r_{i-1}}^{r_i} \frac{\partial c_j(r,t)}{\partial t} \cdot 4\pi r^2 dr \\ &= \int_{r_{i-1}}^{r_i} d \left(4\pi D_j r^2 \frac{\partial c_j(r,t)}{\partial r} \right) \\ &= 4\pi D_j r^2 \frac{\partial c_j(r,t)}{\partial r} \Big|_{r_{i-1}}^{r_i} \\ &= -4\pi D_j r_{i-1}^2 \frac{\partial c_j(r,t)}{\partial r} \Big|_{r_{i-1}} + 4\pi D_j r_i^2 \frac{\partial c_j(r,t)}{\partial r} \Big|_{r_i}. \end{aligned} \quad (\text{A.5})$$

To proceed, we assume that the Li ions are uniformly distributed within each finite volume. That is, the Li-ion concentration for the i -th sphere is

$$c_j(r,t) = \frac{Q_{j,i}(t)}{\Delta V_i} \quad \text{for } r_{i-1} < r \leq r_i,$$

where $\Delta V_i = 4\pi(r_i^3 - r_{i-1}^3)/3$. Then, the concentration gradient at r_i can be approximated as

$$\begin{aligned} \frac{\partial c_j(r,t)}{\partial r} \Big|_{r_i} &= \frac{\frac{Q_{j,i+1}(t)}{\Delta V_{i+1}} - \frac{Q_{j,i}(t)}{\Delta V_i}}{\frac{r_{i+1} - r_{i-1}}{2}} \\ &= \frac{Q_{j,i+1}(t)}{\Delta V_{i+1} \Delta r_{i+1}} - \frac{Q_{j,i}(t)}{\Delta V_i \Delta r_{i+1}}, \end{aligned} \quad (\text{A.6})$$

where $\Delta r_{i+1} = (r_{i+1} - r_{i-1})/2$. Then, according to (A.5)-(A.6) and the boundary conditions in (A.2), we obtain

$$\begin{aligned} \dot{Q}_{j,0}(t) &= -\frac{4\pi D_j r_0^2}{\Delta V_0 \Delta r_1} Q_{j,0}(t) + \frac{4\pi D_j r_0^2}{\Delta V_1 \Delta r_1} Q_{j,1}(t), \quad (\text{A.7}) \\ \dot{Q}_{j,i}(t) &= \frac{4\pi D_j r_{i-1}^2}{\Delta V_{i-1} \Delta r_i} Q_{j,i-1}(t) \\ &\quad - 4\pi D_j \left(\frac{r_{i-1}^2}{\Delta V_i r_i} + \frac{r_i^2}{\Delta V_i \Delta r_{i+1}} \right) Q_{j,i}(t) \\ &\quad + \frac{4\pi D_j r_i^2}{\Delta V_{i+1} \Delta r_{i+1}} Q_{j,i+1}(t), \end{aligned}$$

$$\text{for } 1 \leq i < N, \quad (\text{A.8})$$

$$\begin{aligned} \dot{Q}_{j,N}(t) &= \frac{4\pi D_j r_{N-1}^2}{\Delta V_{N-1} \Delta r_N} Q_{j,N-1}(t) - \frac{4\pi D_j (r_{N-1}^2)}{\Delta V_N \Delta r_N} Q_{j,N}(t) \\ &\pm \frac{4\pi r_N^2}{FS_{p(n)}} I(t). \end{aligned} \quad (\text{A.9})$$

Now let us consider only the positive electrode without loss of generality and suppose that its particle is subdivided into only two finite volumes, the bulk inner domain (core) and the near-surface domain (shell), with $r_0 \gg r_1 - r_0$. This approximates the charge diffusion at the interface between the near-surface area and the inside of the particle. By (A.7)-(A.9), we have

$$\begin{bmatrix} \dot{Q}_{p,0}(t) \\ \dot{Q}_{p,1}(t) \end{bmatrix} = \begin{bmatrix} -\eta_0 & \eta_1 \\ \eta_0 & -\eta_1 \end{bmatrix} \begin{bmatrix} Q_{p,0}(t) \\ Q_{p,1}(t) \end{bmatrix} + \begin{bmatrix} 0 \\ \gamma \end{bmatrix} I(t) \quad (\text{A.10})$$

where $\eta_0 = 4\pi D_p r_0^2 / \Delta V_0 \Delta r_1$, $\eta_1 = 4\pi D_p r_0^2 / \Delta V_1 \Delta r_1$, and $\gamma = 4\pi r_0^2 / FS_p$.

It is seen that $\eta_0 \ll \eta_1$ in (A.10) due to $\Delta V_0 \gg \Delta V_1$ and that $R_s / (R_b + R_s)$ is close to 0 because $R_s \ll R_b + R_s$ in (1). With this observation and comparing (A.10) with (1), we can find that they share an approximately equivalent mathematical form. Thus, from the perspective of physical abstraction, we can associate the shell of the particle with the surface capacitor C_s and the core with the bulk capacitor C_b . Meanwhile, an analogy can be drawn between the voltage difference $V_s - V_b = Q_s / C_s - Q_b / C_b$ and the gradient of the Li-ion concentration in the two finite volumes, which is expressed as $Q_{p,1} / \Delta V_1 - Q_{p,0} / \Delta V_0$. This finding justifies the use of the voltage difference in Sections II and III.

REFERENCES

- [1] Electric Drive Transportation Association. (2015, May) Cumulative U.S. plug-in vehicle sales. [Online]. Available: <http://www.electricdrive.org/index.php?ht=d/sp/i/20952/pid/20952>
- [2] D. Domenico, A. Stefanopoulou, and G. Fiengo, "Lithium-ion battery state of charge and critical surface charge estimation using an electrochemical model-based extended Kalman filter," *ASME Journal of Dynamic Systems, Measurement, and Control*, vol. 132, no. 6, pp. 061302–061302–11, 2010.
- [3] H. Fang, Y. Wang, Z. Sahinoglu, T. Wada, and S. Hara, "State of charge estimation for lithium-ion batteries: An adaptive approach," *Control Engineering Practice*, vol. 25, pp. 45–54, 2014.
- [4] Y. Wang, H. Fang, Z. Sahinoglu, T. Wada, and S. Hara, "Adaptive estimation of the state of charge for lithium-ion batteries: Non-linear geometric observer approach," *IEEE Transactions on Control Systems Technology*, 2015, in press.
- [5] T. Kim, Y. Wang, H. Fang, Z. Sahinoglu, T. Wada, S. Hara, and W. Qiao, "Model-based condition monitoring for lithium-ion batteries," *Journal of Power Sources*, vol. 295, pp. 16–27, 2015.
- [6] H. Fang, X. Zhao, Y. Wang, Z. Sahinoglu, T. Wada, S. Hara, and R. A. de Callafon, "Improved adaptive state-of-charge estimation for batteries using a multi-model approach," *Journal of Power Sources*, vol. 254, pp. 258–267, 2014.
- [7] K. A. Smith, C. D. Rahn, and C. Y. Wang, "Model-based electrochemical estimation and constraint management for pulse operation of lithium ion batteries," *IEEE Transactions on Control Systems Technology*, vol. 18, no. 3, pp. 654–663, 2010.
- [8] A. Bartlett, J. Marcicki, S. Onori, G. Rizzoni, X. G. Yang, and T. Miller, "Electrochemical model-based state of charge and capacity estimation for a composite electrode lithium-ion battery," *IEEE Transactions on Control Systems Technology*, vol. 24, no. 2, pp. 384–399, 2016.
- [9] S. Dey, B. Ayalew, and P. Pisu, "Nonlinear robust observers for state-of-charge estimation of lithium-ion cells based on a reduced electrochemical model," *IEEE Transactions on Control Systems Technology*, vol. 23, no. 5, pp. 1935–1942, 2015.
- [10] M. Scott, N. A. Chaturvedi, and K. Miroslav, "Adaptive partial differential equation observer for battery state-of-charge/state-of-health estimation via an electrochemical model," *ASME Journal of Dynamic Systems, Measurement, and Control*, vol. 136, no. 1, 2013.
- [11] X. Lin, H. Perez, J. Siegel, A. Stefanopoulou, Y. Li, R. Anderson, Y. Ding, and M. Castanier, "Online parameterization of lumped thermal dynamics in cylindrical lithium ion batteries for core temperature estimation and health monitoring," *IEEE Transactions on Control Systems Technology*, vol. 21, no. 5, pp. 1745–1755, 2013.
- [12] B. Suthar, V. Ramadesigan, S. De, R. D. Braatz, and V. R. Subramanian, "Optimal charging profiles for mechanically constrained lithium-ion batteries," *Physical Chemistry Chemical Physics*, vol. 16, no. 1, pp. 277–287, 2013.
- [13] R. Spotnitz, "Simulation of capacity fade in lithium-ion batteries," *Journal of Power Sources*, vol. 113, no. 1, pp. 72–80, 2003.
- [14] H. Bergveld, W. Kruijt, and P. Notten, *Battery Management Systems: Design by Modeling*. Springer, 2002.
- [15] H. A. Catherino, F. F. Feres, and F. Trinidad, "Sulfation in lead-acid batteries," *Journal of Power Sources*, vol. 129, no. 1, pp. 113–120, 2004.
- [16] K. Young, C. Wang, L. Wang, and K. Strunz, "Electric vehicle battery technologies," in *Electric Vehicle Integration into Modern Power Networks*, R. Garcia-Valle and J. P. Lopes, Eds. Springer, 2012.
- [17] C. D. Rahn and C.-Y. Wang, *Battery Systems Engineering*. Wiley, 2013.
- [18] Y. Wong, W. Hurley, and W. W. "Charge regimes for valve-regulated lead-acid batteries: Performance overview inclusive of temperature compensation," *Journal of Power Sources*, vol. 183, no. 2, pp. 783–791, 2008.
- [19] L. T. Lam, H. Ozgun, O. V. Lim, J. A. Hamilton, L. H. Vu, D. G. Vella, and D. A. J. Rand, "Pulsed-current charging of lead/acid batteries — a possible means for overcoming premature capacity loss?" *Journal of Power Sources*, vol. 53, no. 2, pp. 215–228, 1995.
- [20] B. K. Purushothaman and U. Landau, "Rapid charging of lithium-ion batteries using pulsed currents: A theoretical analysis," *Journal of The Electrochemical Society*, vol. 153, no. 3, pp. A533–A542, 2006.
- [21] A. Aryanfar, D. Brooks, B. V. Merinov, W. A. Goddard, A. J. Colussi, and M. R. Hoffmann, "Dynamics of lithium dendrite growth and inhibition: Pulse charging experiments and Monte Carlo calculations," *The Journal of Physical Chemistry Letters*, vol. 5, no. 10, pp. 1721–1726, 2014.
- [22] R. Klein, N. Chaturvedi, J. Christensen, J. Ahmed, R. Findeisen, and A. Kojic, "Optimal charging strategies in lithium-ion battery," in *Proceedings of American Control Conference*, 2011, pp. 382–387.
- [23] J. Yan, G. Xu, H. Qian, and Z. Song, "Model predictive control-based fast charging for vehicular batteries," *Energies*, pp. 1178–1196, 2011.
- [24] H. Perez, N. Shahmohammadhamedani, and S. Moura, "Enhanced performance of li-ion batteries via modified reference governors and electrochemical models," *IEEE/ASME Transactions on Mechatronics*, vol. 20, no. 4, pp. 1511–1520, 2015.
- [25] M. Torchio, N. A. Wolff, D. M. Raimondo, L. Magni, U. Krewer, R. B. Gopaluni, J. A. Paulson, and R. D. Braatz, "Real-time model predictive control for the optimal charging of a lithium-ion battery," in *Proceedings of American Control Conference*, 2015, pp. 4536–4541.
- [26] J. Liu, G. Li, and H. K. Fathy, "Efficient lithium-ion battery model predictive control using differential flatness-based pseudospectral methods," in *Proceedings of ASME 2015 Dynamic Systems and Control Conference*, 2015, p. V001T13A005.
- [27] R. Wai and S. Jhung, "Design of energy-saving adaptive fast-charging control strategy for Li-Fe-PO4 battery module," *IET Power Electronics*, vol. 5, no. 9, pp. 1684–1693, 2012.
- [28] T. Wang and C. G. Cassandras, "Optimal control of batteries with fully and partially available rechargeability," *Automatica*, vol. 48, no. 8, pp. 1658–1666, 2012.
- [29] F. L. Lewis, D. L. Vrabie, and V. L. Syrmos, *Optimal Control*, 3rd ed. Wiley, 2012.
- [30] T. Duncan, L. Guo, and B. Pasik-Duncan, "Adaptive continuous-time linear quadratic Gaussian control," *IEEE Transactions on Automatic Control*, vol. 44, no. 9, pp. 1653–1662, 1999.

- [31] T. Duncan, "Linear-exponential-quadratic gaussian control," *IEEE Transactions on Automatic Control*, vol. 58, no. 11, pp. 2910–2911, 2013.
- [32] J. H. Lee, K. S. Lee, and W. C. Kim, "Model-based iterative learning control with a quadratic criterion for time-varying linear systems," *Automatica*, vol. 36, no. 5, pp. 641 – 657, 2000.
- [33] V. H. Johnson, A. A. Pesaran, and T. Sack, "Temperature-dependent battery models for high-power lithium-ion batteries," in *Proceedings of 17th Electric Vehicle Symposium*, 2000.
- [34] V. H. Johnson, "Battery performance models in ADVISOR," *Journal of Power Sources*, vol. 110, no. 2, pp. 321–329, 2002.
- [35] M. Sitterly, L. Y. Wang, G. Yin, and C. Wang, "Enhanced identification of battery models for real-time battery management," *IEEE Transactions on Sustainable Energy*, vol. 2, no. 3, pp. 300–308, 2011.
- [36] A. Seaman, T.-S. Dao, and J. McPhee, "A survey of mathematics-based equivalent-circuit and electrochemical battery models for hybrid and electric vehicle simulation," *Journal of Power Sources*, vol. 256, pp. 410–423, 2014.
- [37] X.-Z. Yuan, C. Song, H. Wang, and J. Zhang, "EIS equivalent circuits," in *Electrochemical Impedance Spectroscopy in PEM Fuel Cells*. Springer, 2010, pp. 139–192.
- [38] D. Knutsen and O. Willén, "A study of electric vehicle charging patterns and range anxiety," Uppsala University, Tech. Rep., 2013.
- [39] T. Markel and A. Simpson, "Plug-in hybrid electric vehicle energy storage system design," in *Advanced Automotive Battery Conference*, 2006.
- [40] M. B. Pinsona and M. Z. Bazant, "Theory of SEI formation in rechargeable batteries: Capacity fade, accelerated aging and lifetime prediction," *Journal of the Electrochemical Society*, vol. 160, no. 2, pp. A243–A250, 2013.
- [41] W. H. Woodford IV, "Electrochemical shock: Mechanical degradation of ion-intercalation materials," Ph.D. dissertation, Massachusetts Institute of Technology, 2013.
- [42] T. M. Bandhauer, S. Garimella, and T. F. Fuller, "A critical review of thermal issues in lithium-ion batteries," *Journal of the Electrochemical Society*, vol. 158, no. 3, pp. R1–R25, 2011.
- [43] A. E. Bryson, Jr. and Yu-Chi Ho, *Applied Optimal Control*. Taylor & Francis Group, 1975.
- [44] N. Chaturvedi, R. Klein, J. Christensen, J. Ahmed, and A. Kojic, "Algorithms for advanced battery-management systems," *IEEE Control Systems*, vol. 30, no. 3, pp. 49–68, 2010.
- [45] S. Santhanagopalan, Q. Guo, P. Ramadass, and R. E. White, "Review of models for predicting the cycling performance of lithium ion batteries," *Journal of Power Sources*, vol. 156, no. 2, pp. 620–628, 2006.